



# CHORUS

This is the accepted manuscript made available via CHORUS. The article has been published as:

## Medium-range atomic correlation in simple liquids. II. Theory of temperature dependence

Takeshi Egami and Chae Woo Ryu

Phys. Rev. E **104**, 064110 — Published 9 December 2021

DOI: [10.1103/PhysRevE.104.064110](https://doi.org/10.1103/PhysRevE.104.064110)

Notice of Copyright:

*This manuscript has been authored by UT-Battelle, LLC under Contract No. DE-AC05-00OR22725 with the U.S. Department of Energy. The United States Government retains and the publisher, by accepting the article for publication, acknowledges that the United States Government retains a non-exclusive, paid-up, irrevocable, world-wide license to publish or reproduce the published form of this manuscript, or allow others to do so, for United States Government purposes. The Department of Energy will provide public access to these results of federally sponsored research in accordance with the DOE Public Access Plan (<http://energy.gov/downloads/doe-public-access-plan>). [Only for the current manuscript; not to be printed in the publication]*

## **Medium-Range Atomic Correlation in Simple Liquid II:**

### **Theory of Temperature Dependence**

Takeshi Egami<sup>1,2,3</sup> and Chae Woo Ryu<sup>1</sup>

<sup>1</sup>Department of Materials Science and Engineering, University of Tennessee, Knoxville,  
Tennessee 37996, USA

<sup>2</sup>Department of Physics and Astronomy, University of Tennessee, Knoxville, Tennessee 37996,  
USA

<sup>3</sup>Materials Sciences and Technology Division, Oak Ridge National Laboratory, Oak Ridge,  
Tennessee 37831, USA

Corresponding author: Takeshi Egami ([egami@utk.edu](mailto:egami@utk.edu))

ORCID identifier: T. Egami (0000-0002-1126-0276), C. W. Ryu (0000-0003-1588-4868)

#### **Abstract**

The spatial atomic correlations in liquids and glasses extend often significantly beyond the nearest neighbors. Such correlations, called the medium-range order (MRO), affect many physical properties, but their nature is not well-understood. In this article the variation of the MRO with temperature is calculated based upon the concept of the atomic-level pressure, focusing on simple liquids, such as metallic liquids. It is shown that the structural coherence length that characterizes MRO follows the Curie-Weiss law with a negative Curie temperature as observed by experiment and simulation. It is also shown that the glass transition is induced by freezing of the MRO, rather than the freezing of the nearest neighbor shell. The implications of these results are discussed.

## I. Introduction

The atomic structure of liquid and glass is usually described by the atomic pair-distribution function (PDF),  $g(r)$ ,

$$g(r) = \frac{1}{4\pi N \rho_0 r^2} \sum_{i,j} \left\langle \delta(r - |\mathbf{r}_i - \mathbf{r}_j|) \right\rangle, \quad (1)$$

where  $\mathbf{r}_i$  is the atomic position of the  $i$ -th atom,  $N$  is the number of atoms in the system,  $\rho_0$  is the average number density of atoms, and  $\langle \dots \rangle$  denotes thermal and ensemble average [1 – 3]. The PDF depicts the distribution of distances between two atoms. The PDF can be determined by x-ray or neutron diffraction measurement through the Fourier-transformation of the structure function,  $S(Q)$ , where  $Q$  is the momentum transfer of scattering [1 – 3]. Even though some key properties depend on higher-order correlation functions [4, 5], the PDF is widely used in describing the structure because it is a convenient structural descriptor which can be experimentally determined with high accuracy. The PDF is the same-time correlation function, thermal average of snapshots, and does not contain information on dynamics. But it sufficiently characterizes supercooled liquid with relatively slow dynamics, whereas full description of high-temperature liquid requires the knowledge of dynamic correlation functions, such as the Van Hove function [6, 7].

The PDF shows many peaks indicating shell-like structures around an atom. The first peak describes the short-range order (SRO) in the nearest neighbor shell, whereas the peaks beyond the first peak depict the medium-range order (MRO). Ornstein and Zernike were the first to propose a scheme to connect the SRO with the MRO through a self-consistency equation [8]. Slightly different approaches were suggested later by others [2, 3, 9, 10], but all these approaches are based on the idea that the MRO is **directly related to** the SRO. However, as we discussed elsewhere [11 - 14] there are significant differences in the nature between the SRO and the MRO, particularly in the supercooled and glassy states. For instance, the MRO freezes at the glass transition, whereas the SRO does not, **as shown in Part I of this paper** [14]. Even though they are related, they are sufficiently distinct so that the behavior of the MRO cannot be readily predicted from the SRO alone. **The problems with the Ornstein-Zernike (OZ) theory which directly relate the MRO to the SRO in describing supercooled liquid state are well-known, because it is based on the mean-field approximation and higher-order correlations are neglected [3].** In this article we propose an

alternative approach to elucidate the MRO and its temperature dependence down to the glass transition, based on the concept of the structurally coherent ideal glass state [12, 15] and the atomic-level pressure fluctuations [16, 17]. We primarily focus on simple liquids with spherical interatomic potentials, such as metallic liquids.

## II. Short- and medium-range order in liquid and glass

The first peak of the PDF describes the distribution of the nearest neighbor distances from a central atom, which reflects the atomic sizes of the constituent elements and the nature of chemical bonding among them, as well as quantum and thermal fluctuations. In liquids and glasses the number of neighboring atoms for each atom, the local coordination number, varies from site to site. The average coordination number,  $\bar{N}_C$ , is given by the integration over the first peak of the PDF,

$$\bar{N}_C = 4\pi\rho_0 \int_{1st\ peak} g(r)r^2 dr. \quad (2)$$

For simple liquids with dense-random-packed (DRP) structure, such as metallic liquids, the value of  $\bar{N}_C$  is 12 – 14 [18, 19]. At longer distances the PDF oscillates around unity, and its amplitude,  $|g(r)-1|$ , exponentially decays with distance as,

$$|g(r)-1| \approx \frac{\exp(-r/\xi_s)}{r}, \quad (3)$$

where  $\xi_s$  is the structural coherence length which characterizes the MRO.

This form was suggested by Ornstein and Zernike through their self-consistency equation [8]. However, it is possible to arrive at this form from a more general point of view, **as discussed in Part I of this paper.** For crystalline materials the reduced PDF,  $G(r) = 4\pi r \rho_0 [g(r)-1]$ , has persistent oscillations with similar amplitudes up to macroscopic distances [20], because at large distances each peak in  $g(r)$  does not represent a single crystallographic distance, but it represents the number of atoms. This argument applies equally well to liquids and glasses. At large  $r$  the width of the higher-order peaks in  $g(r)$  is of the order of 1 Å, much wider than the typical phonon

amplitudes which are of the order of 0.1 Å. Therefore, the peaks in  $g(r)$  do not represent individual atomic distances, but instead they describe more coarse-grained local density fluctuations [11]. Then, starting from an imaginary state with long-range density correlation,  $G(r)$  should decay because of randomness in the structure of liquid as,

$$G(r) = G_0(r) \exp\left(-\frac{r}{\xi_s(T)}\right), \quad (4)$$

reproducing eq. (3). Here  $G_0(r)$  describes the state with the limit of  $\xi_s \rightarrow \infty$ , the structurally coherent ideal glass state with long-range density correlation, and has persistent oscillations [15]. Interestingly we were able to create a model with such features for Pd<sub>42.5</sub>Ni<sub>7.5</sub>Cu<sub>30</sub>P<sub>20</sub> alloy liquid [15] with the Reverse Monte-Carlo (RMC) method [21], using the experimentally determined  $G(r)$  as a starting point.

It was found that above the glass transition temperature,  $T_g$ ,  $\xi_s(T)$  obeys the Curie-Weiss law for temperature dependence,

$$\frac{\xi_s(T)}{a} = C \frac{T_g}{T - T_{IG}} \quad (T > T_g), \quad (5)$$

where  $a$  is the average nearest neighbor distance,  $T_{IG}$  is the ideal glass temperature where  $\xi_s(T)$  diverges, and is negative for all metallic liquids we studied [15]. Because  $\xi_s$  is linearly related to  $S(Q_1)$ , where  $Q_1$  is the position of the first maximum in  $S(Q)$  [12],  $S(Q_1) - 1$  also follows the Curie-Weiss law [15]. The Curie-Weiss behavior of  $S(Q_1)$  was predicted by the Ornstein-Zernike (OZ) theory at a high-temperature limit [22]. However, in this case the Curie temperature is positive for a system with an attractive potential, whereas our results show it is negative for all metallic liquids studied [15]. Furthermore, according to the OZ theory, the Fourier-transform of the MRO structure function,  $h(\mathbf{Q}) = S(\mathbf{Q}) - 1$ , is given by,

$$h(\mathbf{Q}) = \frac{c(\mathbf{Q})}{1 - \rho_0 c(\mathbf{Q})}. \quad (6)$$

where  $c(\mathbf{Q})$  describes the SRO [3, 8]. Therefore, a continuous variation of  $c(\mathbf{Q})$  with temperature through  $T_g$  as observed by experiment should result in a continuous variation of  $h(\mathbf{Q})$  as well, whereas  $S(Q_1)$  shows a sharp change in its temperature dependence at  $T_g$  [15]. Thus, the OZ theory

cannot explain the important difference between the SRO and MRO with respect to the temperature dependence through  $T_g$  as observed by experiment and simulation [14]. The apparent failure of the OZ theory is partly because the high-temperature approximation does not work for supercooled liquid. Also, the validity of the mean-field approximation in the OZ theory is questionable for supercooled liquid in which atoms are dynamically strongly correlated. In the following we propose an alternative theory which explains the Curie-Weiss behavior of  $\xi_s(T)$  with a positive Curie temperature based upon the concept of the atomic-level pressure.

### III. Results

#### A. Structurally coherent ideal glass state

The  $G_0(r)$  in eq. (4) describes the state extrapolated in the limit of  $\xi_s \rightarrow \infty$ . This state has long-range correlation with no positional order. We call it the structurally coherent ideal liquid (glass) [15]. The  $G_0(r)$  can be obtained from the  $G(r)$  determined by experiment as  $G_0(r) = G(r) \exp(r/\xi_s)$ . Fig. 1 shows the  $G(r)$  of amorphous Fe at  $T_g$  (1000K) obtained by simulation, and the corresponding  $G(r)$  of the structurally coherent ideal glass. The simulation was carried out by using the LAMMPS software [23] with the modified Johnson potential for Fe [24] for a model of 16000 atoms with periodic boundary conditions. The model was equilibrated at 2000K and cooled with the rate of 2 K/ps to avoid crystallization. The model of the structurally coherent ideal glass with 54000 atoms with periodic boundary conditions was obtained by the RMC method [21] to fit to  $G_0(r)$ , with the constraint of the minimum atomic separation of 2.0 Å. The amplitude of oscillations in  $G(r)$  for the model obtained by the RMC is smaller than that of  $G_0(r)$ , but the periodicities are the same [15]. The MRO portion of  $G(r)$  is approximately given by,

$$G_{MRO}(r, T) \approx A_{MRO}(T) a \sin(Q_{MRO} r + \delta_{MRO}(T)) \exp\left(-\frac{r}{\xi_s(T)}\right), \quad r > r_{cutoff}. \quad (7)$$

where  $a$  is the nearest neighbor distance defined by the first maximum in the PDF,  $A_{MRO}(T)$  is the amplitude of the MRO oscillation,  $\delta_{MRO}(T)$  is the phase factor, and  $r_{cutoff}$  is the position of the first minimum of the PDF beyond the first peak. Both  $A_{MRO}(T)$  and  $\delta_{MRO}(T)$  show only weak variations

with temperature [14].  $Q_{\text{MRO}}$  is almost identical to  $Q_1$ . The  $S(Q)$  of the structurally coherent ideal glass state ( $\xi_s \rightarrow \infty$ ) has a single Bragg sphere at  $Q_{\text{MRO}}$  [15]. The Curie-Weiss law, eq. (5), shows that the system is driven to the structurally coherent ideal glass state as temperature is reduced. The driving force to increase the coherence will be discussed elsewhere. We will assume that the structurally coherent ideal glass state represents the ground state of the system, although this state exists only in extrapolation, and in reality various frustration factors prevent the system from reaching this state, **just as the frustrated ideal states assumed by other theories [25 – 27]**. We will conceptually start from this state, and then consider deviations from this state due to frustration and thermal excitations.

## B. Deviation from the structurally coherent ideal glass state and the MRO

We assume that the imaginary structurally coherent ideal glass state as the ground state of the system. As temperature is increased thermal density fluctuations reduce the coherence length as in eq. (4). Thermal volume strain at an atom,  $i$ , is given by,

$$\varepsilon_{V,i} = 3\varepsilon_{r,i} = 3\frac{u_{r,i}}{a}, \quad u_{r,i} = \frac{1}{N_{C,i}} \sum_j u_{ij}, \quad (8)$$

where  $N_{C,i}$  is the number of nearest neighbors of  $i$ -th atom,  $u_{ij}$  is the deviation in the distance between the center atom  $i$  to the nearest neighbor atom,  $j$ , from the distance in the structurally coherent ideal glass state, and  $a$  is the average nearest neighbor distance. The second moment of the average is,

$$\langle (\varepsilon_V)^2 \rangle = \frac{9}{N_C^2} \left\langle \sum_j (u_{ij})^2 \right\rangle = \frac{9}{N_C} \langle (\varepsilon_R)^2 \rangle, \quad (9)$$

where

$$\varepsilon_R = \left( \frac{1}{N_C} \sum_j (u_{ij})^2 \right)^{\frac{1}{2}}. \quad (10)$$

describes the root-mean-square magnitude of local fluctuations in the near neighbor distance which varies with time. For simple liquids  $\bar{N}_C = 4\pi$  [28]. If we introduce volume, or density, fluctuation

described by  $\varepsilon_R$  to the structurally coherent ideal glass state, the decay of  $G(r)$  from  $r$  to  $r + R$ , where  $R = 2\pi/Q_{MRO}$ , is given by

$$\frac{G(r+R)}{G(r)} = \frac{\langle \sin(Q_{MRO}(r+R(1+\varepsilon_R))) \rangle}{\sin(Q_{MRO}r)} = \exp\left(-\frac{\langle (Q_{MRO}R\varepsilon_R)^2 \rangle}{2}\right) = \exp\left(-\frac{R}{\xi_s}\right), \quad (11)$$

Thus,

$$\frac{1}{\xi_s} = \frac{Q_{MRO}^2 R \langle (\varepsilon_R)^2 \rangle}{2} = \frac{\pi \bar{N}_C}{9} Q_{MRO} \langle (\varepsilon_V)^2 \rangle. \quad (12)$$

Now the nearest neighbor distance,  $a$ , is defined by the first peak in eq. (7). Then, neglecting the phase factor,  $\delta_{MRO}$ , which is small,  $aQ_{MRO} = 5\pi/2$ ,

$$\frac{a}{\xi_s} = \frac{10\pi^3}{9} \langle \varepsilon_V^2 \rangle. \quad (13)$$

This equation relates the coherence length of the MRO to the volume fluctuation at the atomic level.

### C. Atomic-level stress and strain

We now calculate the volume fluctuation at the atomic level using the atomic-level stresses tensor for an atom  $i$ ,  $\bar{\bar{\sigma}}_i$ . It is defined by

$$\sigma_i^{\alpha\beta} = \frac{1}{V_i} \sum_j f_{ij}^\alpha r_{ij}^\beta, \quad (14)$$

where  $\alpha$  and  $\beta$  refer to Cartesian indices,  $V_i$  is the local atomic volume of atom  $i$ , and  $f_{ij}^\alpha$  and  $r_{ij}^\beta$  are the  $\alpha$  and  $\beta$  components of the two-body force and distance between atoms  $i$  and  $j$  [16, 17].

Its trace gives the atomic-level pressure

$$p_i = \frac{1}{3} (\sigma_i^{xx} + \sigma_i^{yy} + \sigma_i^{zz}). \quad (15)$$

whereas five other combinations give the shear, or deviatoric, stresses,  $\tau_{m,i}$ ,  $m = 1 \sim 5$ . Because the bulk of the two-body forces originates from the nearest neighbors the atomic-level stresses characterize the configuration of the nearest neighbors [17]. For instance, the atomic volume strain,

$$\varepsilon_{V,i} = \frac{P_i}{B}, \quad (16)$$

where  $B$  is bulk modulus, describes the local atomic volume variation compared to the equilibrium atomic volume. There are six stress components in each stress tensor, but because  $f_{ij}^\alpha = -f_{ji}^\alpha$  the contribution from each bond  $\{i, j\}$  is counted twice, so the total number of variables in the system of  $N$  particles is  $3N$ , equal to the degree of freedom of the system. This means that it is possible to describe the atomic dynamics in terms of the dynamics of the atomic-level stresses, if excitations are localized. Indeed, in the liquid state the atomic-level stresses follow the equipartition theorem,

$$\frac{\langle p^2 \rangle}{2B} = \frac{\langle \tau^2 \rangle}{2G} = \frac{k_B T}{4}, \quad (17)$$

where  $G$  is shear modulus [29, 30].

The principal origin of the atomic-level pressure is the atomic size mismatch [17, 28]. If we place an atom to an atomic site in a solid which is smaller than the atomic size, this atom will be under compressive stress. To evaluate this effect correctly, however, we have to consider the accommodation effect by the surrounding atoms. For instance, in an icosahedral cluster the distance between the center and the apex is shorter than the apex-apex distance by 4.9%. This means that in order to form an icosahedron with hard spheres, we have to use a sphere at the center which is smaller by  $\Delta x = 0.098$  than the 12 spheres on the peripheral sites. If we use 13 soft spheres with the same size, we have to compress the central sphere by  $\varepsilon_V^T = 1 - (1 - \Delta x)^3 = 0.266$  in volume strain to place it at the center of the icosahedron without straining other atoms. The  $\varepsilon_V^T$  is called the transformation strain [31]. At this moment all the strain is in the center atom, whereas the atoms at the peripheral sites has no strain. To reduce the total energy the strain on the central atom needs to be relaxed by  $\varepsilon_V^R$  and other atoms need to be strained to accommodate the relaxation. For an icosahedral cluster of 13 atoms interacting via the modified Johnson potential this strain was calculated to be  $\varepsilon_V^R = 0.141$ , after consideration of the secondary accommodation of the icosahedral cluster by surrounding elastic medium (see Appendix 1).

This elastic accommodation by the neighbor atoms can be modeled well by the elastic inclusion theory by Eshelby [31]. In this theory an elastic sphere is inserted into an elastic medium with a spherical hole. The size of the inserted sphere, inclusion, does not match the size of the hole. In order to match the size of the hole the size of the inclusion has to be changed by a volume strain,  $\varepsilon_V^T$ . After insertion the system is relaxed so that the strain in the inclusion can be partly accommodated by the surrounding elastic medium. According to the Eshelby theory the strain on the inclusion after relaxation is given by

$$\varepsilon_V^I = \frac{\varepsilon_V^T}{K_\alpha}, \quad (18)$$

where

$$K_\alpha = \frac{3(1-\nu)}{2(1-2\nu)}, \quad (19)$$

and  $\nu$  is Poisson's ratio, and the relaxation strain,  $\varepsilon_V^R = \varepsilon_V^T - \varepsilon_V^I$  is given by

$$\varepsilon_V^R = \left(1 - \frac{1}{K_\alpha}\right) \varepsilon_V^T. \quad (20)$$

The total energy is,

$$E = \frac{BV}{2K_\alpha} (\varepsilon_V^T)^2. \quad (21)$$

For the 13 icosahedral cluster of Fe atoms interacting with the modified Johnson potential,  $\nu = 0.25$ ,  $\varepsilon_V^T = 0.266$ . We obtain  $\varepsilon_V^R = 0.148$  according to eq. (20), which only slightly (by 5%) overestimates what is calculated for the icosahedral cluster embedded in an elastic medium, 0.141. Thus, the Eshelby theory is quite reliable in evaluating the atomic-level stresses due to the atomic size mismatch including the accommodation by the neighboring atoms, even though the atomic systems are not an elastic continuum as assumed by Eshelby [17].

#### D. Atomic-level pressure in liquid

In liquid the local structure has a wide variety in topology [18]. However, the atomic-level pressure is primarily dependent on the local coordination number rather than the detailed topology [17, 32]. The relation between the coordination number,  $N_C$ , and the average atomic-level pressure for a specific value of  $N_C$  can be calculated in the following way. If we place an  $A$  atom with the radius  $r_A$  in the liquid of  $B$  atoms with the radius of  $r_B$ , the average coordination number is given by [28],

$$N_C(x) = 4\pi \left(1 - \frac{\sqrt{3}}{2}\right) (1+x) \left(1+x + \sqrt{x(x+2)}\right). \quad (22)$$

where  $x = r_A/r_B$ . If we replace the  $A$  atom with a  $B$  atom, it does not fit because of the difference in size. This mismatch produces the atomic-level pressure. The atomic size is not inherent to each element but depends on bonding and chemical environment [33], but here we neglect these effects and focus on purely geometric argument.

First, we start with the structurally coherent ideal glass state given by eq. (7). Even though this glass has long-range structural coherence, its local structure is quite diverse with distributed coordination numbers [15]. Thus, if we try to form this glass with a single element, atoms do not fit the atomic site. To make an atom fit snug into each site with the coordination number  $N_C$ , we have to compress or expand the atom by the volume strain,

$$\varepsilon_v^T = \frac{3}{2} \Delta x = 3(3 - 2\sqrt{3}) \left(\frac{N_C}{4\pi} - 1\right). \quad (23)$$

as derived from the derivative of eq. (22) evaluated at  $x = 1$  (see Appendix 2). The pressure is given by  $p^T = B \varepsilon_v^T$ . At this moment all the strain is in the center atom, but to reduce the total energy the strain on the central atom needs to be relaxed by  $\varepsilon_v^R$  and the matrix needs to be strained to accommodate the relaxation, by eq. (20). Now, to create the state with  $\xi_s \rightarrow \infty$ , the structurally coherent ideal glass state, atoms have to be compressed or expanded with  $\varepsilon_v^T$  to fit the structure. After the strain  $\varepsilon_v^T$  is locally relaxed by  $\varepsilon_v^R$  by straining the neighbors, the structure is deviated from the structurally coherent ideal glass state and loses long-range coherence. Therefore,  $\varepsilon_v^R$  is the volume strain that characterizes the deviation from the structurally coherent ideal glass state. Thus,

$$\frac{a}{\xi_s} = \frac{10\pi^3}{9} \left\langle (\varepsilon_v^R)^2 \right\rangle. \quad (24)$$

## E. Variation of the MRO with temperature

Now there are two kinds of strain. The first is the misfit strain,  $\varepsilon_V^{T,mf}$ , that originates from the misfit of the atomic size to the structurally coherent ideal glass state as we discussed above, which depends on chemical composition. The second is thermal strain due to thermal atomic fluctuations,  $\varepsilon_V^{T,th}$ . Because the misfit strain is static whereas thermal strain is dynamic with zero average,

$$\langle (\varepsilon_V^T)^2 \rangle = \langle (\varepsilon_V^{T,mf})^2 \rangle + \langle (\varepsilon_V^{T,th})^2 \rangle. \quad (25)$$

For the thermal strain, through the equipartition theorem for  $T > T_g$  [29, 30] we find,

$$\langle E_{th} \rangle = \frac{k_B T}{4}, \quad (26)$$

$$k_B T = \frac{2BV}{K_\alpha} \langle (\varepsilon_V^{T,th})^2 \rangle, \quad (27)$$

$$\langle (\varepsilon_V^{R,th})^2 \rangle = \frac{(K_\alpha - 1)^2}{K_\alpha} \frac{k_B T}{2BV}. \quad (28)$$

Thus, the strain which determines the MRO through eq. (23) is given by,

$$\langle (\varepsilon_V^R)^2 \rangle = \langle (\varepsilon_V^{R,mf})^2 \rangle + \langle (\varepsilon_V^{R,th})^2 \rangle = \frac{9}{10\pi^3} \frac{a}{\xi_s} = \frac{(K_\alpha - 1)^2}{K_\alpha} \frac{k_B (T - T_{IG})}{2BV}. \quad (29)$$

for  $T > T_g$  where

$$\langle (\varepsilon_V^{R,mf})^2 \rangle = -\frac{(K_\alpha - 1)^2}{K_\alpha} \frac{k_B T_{IG}}{2BV}. \quad (30)$$

Therefore,  $T_{IG} < 0$ . Thus,

$$\frac{\xi_s(T)}{a} = C \frac{T_g}{T - T_{IG}}, \quad (31)$$

where

$$C = \frac{9}{10\pi^3} \frac{K_\alpha}{(K_\alpha - 1)^2} \frac{2BV}{k_B T_g}, \quad (32)$$

which explains the Curie-Weiss law observed for  $\xi(T)$  and  $S(Q_1)$  by diffraction experiment and by simulation [15]. Because  $T_g$  is given by [34],

$$k_B T_g = \frac{2BV}{K_\alpha} (\varepsilon_V^{T,crit})^2, \quad (33)$$

where  $\varepsilon_V^{T,crit}$  is the universal critical transformation strain for glass transition, we obtain,

$$C = \left( \frac{9}{10\pi^3} \right) \frac{1}{(\varepsilon_V^{T,crit})^2 \left( 1 - \frac{1}{K_\alpha} \right)^2} \quad (34)$$

## F. Comparison with simulation and experiment

We tested our prediction, eq. (29), with MD simulations using the LAMMPS software [23] for systems with 16000/32000 atoms. The test was made firstly with the model by an embedded atom model (EAM) type many-body potential for Fe [35], which was designed to keep the value of  $B$  constant and vary  $G$ . We used this model because it allows to examine the effect of Poisson's ratio without changing composition, thus avoiding the complications due to alloying. The total potential energy is given by,

$$E_{PE} = \sum_i \left[ F(\bar{\rho}_i) + \frac{1}{2} \sum_{j \neq i} \phi(r_{ij}) \right], \quad (35)$$

where  $\phi(r)$  is the two-body potential, and

$$F(\bar{\rho}) = \frac{A}{2} F_0 \bar{\rho} [\ln \bar{\rho} - 1], \quad (36)$$

$$\bar{\rho}_i = \frac{1}{\rho_T} \sum_{j \neq i} \rho(r_{ij}), \quad (37)$$

$$\rho_T = \sum_{j \neq i} \rho(r_{ij}), \quad (38)$$

$$\rho(r) = \exp\left[-\beta\left(\frac{r}{r_0} - 1\right)\right], \quad (39)$$

$$F_0 = -\frac{1}{N} \sum_{i,j \neq i} \rho(r_{ij}) [\ln \rho(r_{ij}) - 1], \quad (40)$$

where  $r_0 \approx a$  [35]. We choose the modified Johnson potential (mJp) [24] as the pair potential  $\phi(r)$ , and  $\beta = 6$ . The coherence length,  $\xi_s(T)$ , and bulk and shear moduli were calculated as a function of temperature for the systems with  $A = 0$  (the original mJp for Fe),  $A = 0.04, 0.08$  and  $0.12$ . The plots of  $a/\xi(T)$  against  $T$  are shown in Fig. 2, for simulation with various values of  $A$ , and are compared to those by eq. (29) using the simulation values for  $T_{IG}$ . Even though we applied the Eshelby theory based on elastic continuum to discrete atomic systems, eq. (29) explains the Curie-Weiss law of the data with excellent agreement for the slope.

The second moment of the volume strain,  $\langle \varepsilon_V^2 \rangle$ , is proportional to  $a/\xi(T)$  via eq. (13), so is linear with temperature as shown in Fig. 3 for the experimental data for  $\text{Pd}_{42.5}\text{Ni}_{7.5}\text{Cu}_{30}\text{P}_{20}$  alloy liquid and the simulation data for various metallic alloy liquids in Ref. 15. We calculated the value of  $C$ , the slope of the Curie-Weiss plot by eq. (32), and compared it in Fig. 4 (a) with the value obtained for the data shown in Figs. 2 and 3. In evaluating eq. (32) we used macroscopic values of elastic moduli, calculated by imposing macroscopic strain by gradually modifying the periodic boundary conditions and relaxing the structure at  $T = 1\text{K}$ . However, the alloys are chemically heterogeneous, and the macroscopic moduli represents the average values for local elasticity. For this reason, the results shown in Fig. 4 (a) indicate small disagreement with the fitted  $C$  values for alloy glasses, even though it works very well for single component glassy Fe. We also determined the effective value of  $K_\alpha$  for the simulation results and calculated the effective Poisson's ratio,  $\nu_{eff}$ . The value of  $\nu_{eff}$  is compared with the calculated value of  $\nu$  in Fig. 4 (b) for the experimental data on  $\text{Pd}_{42.5}\text{Ni}_{7.5}\text{Cu}_{30}\text{P}_{20}$  alloy liquid and the simulation data for various metallic alloy liquids in Ref. 15, in addition to the Fe simulation data using the many-body potential, eq. (35). Overall agreement is excellent, supporting the validity of eq. (29) in explaining the Curie-Weiss law and predicting its slope.

The value of  $\varepsilon_v^{T,crit}$  in eq. (33) determined for experimental data is equal to 0.095 [34]. However, for simulation the effective cooling rate,  $5 \times 10^{10}$  K/s, is much higher than those for experiments. Interestingly, in spite of such large difference in cooling rates, eq. (33) is valid even for simulation if we use a slightly higher value of  $\varepsilon_v^{T,crit}$ , which is equal to 0.105, as shown in Fig. 5.

## IV. Discussion

### A. Structural frustration

Liquids are condensed matter with density comparable to those in the solid state. In some cases, liquids are denser than solids, as in water and ice. The attractive interatomic potential drives cohesion, and results in the condensation of liquid. In the case of metallic or Lennard-Jones (LJ) liquids, maximizing compaction, thus density, is the primary principle for formation of the structure. Local density is maximized for four atoms forming a tetrahedral cluster. But the entire three-dimensional space cannot be filled with tetrahedra, as is well-known as the inherent structural frustration of three-dimensional space, where rules for local space filling and global space filling are not the same [25 – 27].

Here, imposing the long-range order in  $G_0(r)$  resulted in the large varieties in the SRO [15], as an outcome of this frustration. The local strain,  $\varepsilon_v^{T,mf}$ , represents the atomic size mismatch due to the frustration. From eqs. (30), (31) and (33) we obtain,

$$\frac{\xi_s(T_g)}{a} = \frac{C}{1 - T_{IG}/T_g}, \quad (41)$$

$$\frac{T_{IG}}{T_g} = - \frac{\langle (\varepsilon_v^{T,mf})^2 \rangle}{(\varepsilon_v^{T,crit})^2}. \quad (42)$$

The  $\xi_s(T_g)/a$  is related the liquid fragility [36],

$$m = \left. \frac{d \log \eta}{d(T_g/T)} \right|_{T=T_g}, \quad (43)$$

where  $\eta$  is viscosity [37]. Thus, the misfit strain is large for fragile liquid and is small for strong liquid. In Fig. 6  $m$  is compared against  $1/[1 + |T_{IG}/T_g|]^3$  for various metallic liquids. The values of  $m$  are determined by experiment [38 – 43]. A correlation between fragility and the misfit strain is clearly seen. The  $\xi_s(T_g)/a$ , thus the misfit strain, is also related to the ratio,  $w_L/w_G$ , where  $w_L$  and  $w_G$  are the Lorentzian and Gaussian widths when the first peak of  $S(Q)$  is fitted with the Voigt function, which is a hybrid of the Lorentzian and Gaussian peaks. Because the exponential decay, eq. (3), results in the Lorentzian peak shape, we suggest that this ratio characterizes the ideality of the structure [12]. In summary, the misfit strain,  $\varepsilon_V^{T,mf}$ , arises as a consequence of structural frustration, and is small for fragile, more ideal liquid, and large for strong, less ideal liquid.

## B. Relation between MRO and SRO

The stress tensor, eq. (14), has six components, the pressure, the  $\ell = 0$  term in the spherical harmonics representation, and the five shear components, the  $\ell = 2$  terms. Whereas the first peak of  $G(r)$  reflects all six terms, we have shown here that the MRO represents only the pressure fluctuations. There are several reasons for this important difference. The first is that whereas the first peak of the PDF which describes the SRO depicts the atom-atom correlations, or the *point-to-point* correlations, the MRO peaks represents the correlation between the central atom to the coarse-grained density fluctuations, the *point-to-set* correlations [44]. The density fluctuations are controlled by pressure fluctuation. The second reason is that if we describe the structure in terms of the density waves [45, 46], the PDF sees only the longitudinal waves, and not the shear waves [3]. Furthermore, the shear waves are strongly damped, and would not propagate in liquids [2, 3].

We found that in supercooled liquid viscosity is determined by the coherence length of the MRO. The activation energy for viscosity,  $E_a(T)$ ,

$$\eta(T) = \eta_\infty \exp\left(\frac{E_a(T)}{k_B T}\right), \quad (44)$$

is related to  $\xi_s(T)$  through,

$$E_a(T) = E_0 \left( \frac{\xi_s(T)}{a} \right)^3. \quad (45)$$

just above  $T_g$  in  $\text{Pd}_{42.5}\text{Ni}_{7.5}\text{Cu}_{30}\text{P}_{20}$  liquid [15]. Because the glass transition is defined by  $\eta$  reaching  $10^{13}$  poise ( $= 10^{12}$  Pa.s), the glass transition is controlled by  $\xi_s(T)$ , thus by the volume fluctuation,  $\varepsilon_V^{T,th}$ , reaching the critical value,  $\varepsilon_V^{T,crit}$ .

On the other hand, the SRO represented by the height of the first peak of the PDF, is dominated by local shear fluctuations, because there are five shear components in comparison to one component of pressure, and shear modulus,  $G$ , is lower than the bulk modulus,  $B$ , resulting in larger shear strain [17]. Consequently, almost no change in the temperature derivative is seen at  $T_g$  for the height of the first peak of the PDF [14]. This observation, that the SRO dynamics is not frozen in the glassy state below  $T_g$  even though the MRO is frozen, has very significant implications on the properties of simple glasses, as will be discussed elsewhere.

Various models assume high-symmetry atomic clusters, such as an icosahedral cluster, as building blocks to form the MRO by stacking these clusters [47 – 49]. In such models the relevant length-scale for the MRO is the inter-cluster distance, which is a few times the atomic distance, whereas the periodicity of the observed MRO oscillations is comparable to the interatomic distance. Therefore, the MRO discussed here cannot be explained in terms of the building of the SRO clusters. Furthermore, in such models the distribution of the atomic-level strains will be bifurcated, less for the atoms within the clusters and more for those connecting the clusters. But, the distribution of atomic-level stresses shows a single Gaussian distribution, with no evidence of bifurcation [32, 50]. In general, spatially heterogeneous distribution of stresses results in higher total elastic energy and is not preferred. In the present work statistically homogeneous fluctuation of the atomic-level stress is assumed, without assuming any building block.

## V. Conclusion

For a long time, the medium-range order (MRO) in liquid and glass, defined by the atomic correlations beyond the nearest neighbors, has been considered to be a **direct** consequence of the

short-range order (SRO) in the group of the nearest neighbor atoms. Consequently, research efforts focused on relating the properties of liquid and glass directly to the interatomic potential and the SRO. However, mounting evidence suggests that the MRO is distinct in nature from the SRO, and the relationship between them is indirect. This distinction is important because some properties, including viscosity and glass transition, are controlled more by the MRO than by the SRO. In this article we discuss the MRO as it relates to the deviation from the structurally coherent ideal glass state. Focusing on simple liquids, such as metallic liquids, we calculate the temperature dependence of the MRO based upon the concept of the atomic-level pressure. The results provide the theoretical basis for the Curie-Weiss law for the structural coherence length as observed by experiment and simulation.

The temperature dependence of the MRO is quite distinct from that of the SRO, and the freezing of the MRO, not that of the SRO, defines the glass transition. Describing the evolution of the liquid structure with temperature, the elucidation of the glass transition in particular, has been a long-standing question. The theory described here presents a solution supported by experimental and simulation data, and provides an important piece of the puzzle on the origin of the glass transition, at least for simple liquids with spherical pairwise or EAM type potentials, such as most metallic liquids. The extension to more complex liquids, including covalent liquids, is left for future work.

## **Acknowledgment**

The authors thank J. S. Langer for discussion and W. Dmowski for help in the calculation of elastic moduli. This work was supported by the US Department of Energy, Office of Science, Basic Energy Sciences, Materials Sciences and Engineering Division.

## Appendix 1: Eshelby theory

For an icosahedral cluster of 13 Fe atoms interacting with the modified Johnson potential [24], the distance between the central atom and the edge atom is  $R_{CE} = 2.522 \text{ \AA}$  and the edge-edge distance is  $R_{EE} = 2.652 \text{ \AA}$ . Because the equilibrium distance is  $R_0 = 2.622 \text{ \AA}$ , the strain on the center-edge bond is  $\varepsilon_{LC} = (R_{CE} - R_{EE})/R_{EE} = -0.0381$ , thus  $\varepsilon_V^{J,FS} = 1 - (1 + \varepsilon_{LC})^3 = 0.110$  for the center atom. By comparing to  $\varepsilon_V^T = 0.266$ , we obtain  $\varepsilon_V^{R,FS} = 0.156$  for the center atom in a free-standing icosahedral cluster. However, the strain on the edge-edge bond is  $\varepsilon_{LE} = 0.0114$ . This means that the icosahedral cluster has expanded by  $\varepsilon_V^C = 0.0346$  compared to the ideal volume of the icosahedral cluster. In order to reduce the volume of the icosahedral cluster to the ideal volume we have to apply the transformation volume strain to the cluster,  $\varepsilon_V^{T,cluster} = \varepsilon_V^C$ . We then repeat the same Eshelby procedure for the cluster, by compressing it to the ideal volume, placing it in the hole of the elastic medium with the same ideal size, and relaxing the cluster and the medium to minimize the total elastic energy. By eq. (18), we obtain  $\varepsilon_V^{JC} = 0.0154$  for the icosahedral cluster. This has to be added to  $\varepsilon_V^{J,FT}$ . Therefore, the final strain on the inclusion after the cluster is embedded in the elastic medium is,  $\varepsilon_V^J = 0.125$ , and the relaxation strain is  $\varepsilon_V^{RC} = 0.141$ . The value obtained by the Eshelby theory, eq. (20),  $\varepsilon_V^R = 0.148$ , is in the middle between  $\varepsilon_V^{RC} = 0.141$  and  $\varepsilon_V^{R,FS} = 0.156$ .

It should be noted that the elasticity theory of Eshelby is applicable even for liquid, as long as the relaxation time of liquid is longer than the phonon timescale so that liquid behaves like solid as far as elasticity is concerned. For this comparison the Maxwell relaxation time,  $\tau_M = \eta/G_\infty$ , where  $\eta$  is viscosity and  $G_\infty$  is the high-frequency shear modulus, should be compared with the time for phonon to propagate to the nearest neighbor, because most of the Eshelby strain is born by the shell of nearest neighbor atoms. They become equal to each other at the viscosity crossover temperature,  $T_A$  [51]. Therefore, the Eshelby theory is applicable at least at temperatures below  $T_A$ , which is about twice  $T_g$  for metallic liquids [52] and higher for molecular liquids [53].

## Appendix 2: Derivation of eq. (23)

From eq. (22), the ideal value of  $N_C$  for  $x = 1$  is

$$N_C(1) = 4\pi. \tag{A1}$$

Also,

$$\left. \frac{dN_C(x)}{dx} \right|_{x=1} = 2\pi \left( 1 + \frac{2}{\sqrt{3}} \right). \quad (\text{A2})$$

Thus, to the first order,

$$\Delta x = x - 1 = \left. \frac{dx}{dN_C} \right|_{x=1} \Delta N_C, \quad \Delta N_C = N_C(x) - N_C(1) = \left( \frac{N_C}{4\pi} - 1 \right), \quad (\text{A3})$$

To fit a sphere with  $r_B = xr_A$  to the site for  $x = 1$  we have to change the size by  $\Delta x = x - 1$ . Then the  $A$ - $B$  bond length,  $r_A + r_B = (1 + x)r_A$ , has to be compressed to  $2r_A$ . Thus, the Voronoi volume defined by the nearest neighbors has the volume strain,

$$\varepsilon_v^T = \frac{3}{2} \Delta x. \quad (\text{A4})$$

From (A2) – (A4) we derive eq. (23).

## References:

1. B. E. Warren, *X-ray Diffraction* (Addison-Wesley, Reading, 1969).
2. P. A. Egelstaff, *An Introduction to the Liquid State* (First Edition, Academic Press, 1967, Second Edition, Oxford University Press, 1991).
3. J.-P. Hansen, I. R. McDonald, *Theory of Simple Liquids* (Academic Press, 1976, 1986, 2006).
4. S. C. Glotzer, V. N. Novikov and T. B. Schröder, *J. Chem. Phys.* **112**, 509 (2000).
5. S. Albert, Th. Bauer, M. Michl, G. Biroli, J. P. Bouchaud, A. Loidl, P. Lunkenheimer, R. Tourbot, C. Wiertel-Gasquet and F. Ladieu, *Science* **352**, 1308 (2016).
6. L. Van Hove, *Phys. Rev.* **95**, 249 (1954).
7. T. Egami and Y. Shinohara, *J. Chem. Phys.*, **153**, 180902 (2020).
8. L. S. Ornstein and F. Zernike, *Proc. Roy. Netherlands Acad. Arts Sci. (KNAW)* **17**, 793 (1914).
9. J. S. Rowlinson, *Rep. Prog. Phys.* **28**, 169 (1965).
10. J. K. Percus and G. J. Yevick, *Phys. Rev.* **110**, 1 (1958).
11. T. Egami, *Front. Phys.* **8**, 50 (2020).
12. C. W. Ryu, W. Dmowski and T. Egami, *Phys. Rev. E* **101**, 030601(R) (2020).
13. T. Egami and C. W. Ryu, *Front. Chem.* **8**, 579169 (2020).
14. C. W. Ryu and T. Egami, unpublished [EZ11911].
15. C. W. Ryu, W. Dmowski, K. F. Kelton, G. W. Lee, E. S. Park, J. R. Morris and T. Egami, *Sci. Rep.* **9**, 18579 (2019).
16. T. Egami, K. Maeda and V. Vitek, *Phil. Mag. A* **41**, 883 (1980).
17. T. Egami, *Prog. Mater. Sci.* **56**, 637-653 (2011).
18. J. D. Bernal and J. Mason, *Nature* **188**, 910 (1960).

19. G. S. Cargill, III. *Solid State Phys.* **30**, 227 (1975).
20. V. A. Levashov, S. J. L. Billinge and M. F. Thorpe, *Phys. Rev. B* **72**, 024111 (2005).
21. R. L. McGreevy, *J. Phys.: Condens. Matter.* **13**, R877- R913 (2001).
22. S. Chakrabarty and Z. Nussinov, *Phys. Rev. B* **84**, 064124 (2011).
23. S. Plimpton, *J. Comp. Phys.* **117**, 1 (1995) and <http://lammmps.sandia.gov>.
24. D. Srolovitz, K. Maeda, V. Vitek and T. Egami, *Philos. Mag. A* **44**, 847 (1981).
25. D. R. Nelson, *Phys. Rev. B* **28**, 5515 (1983).
26. J. P. Sethna, *Phys. Rev. Lett.* **51**, 2198 (1983).
27. G. Tarjus, S. A. Kivelson, Z. Nussinov and P. Viot, *J. Phys.: Condens. Matter* **17**, R1143 (2005).
28. T. Egami and S. Aur, *J. Non-Cryst. Solids* **89**, 60 (1987).
29. S.-P. Chen, T. Egami and V. Vitek, *Phys. Rev. B* **37**, 2440 (1988).
30. V. A. Levashov, T. Egami, R. S. Aga and J. R. Morris, *Phys. Rev. B* **78**, 064205 (2008).
31. J. D. Eshelby, *Proc. Roy. Soc. London A* **241**, 376 (1957).
32. T. Egami and D. Srolovitz, *J. Phys. F* **12**, 2141 (1982).
33. D. M. Nicholson, Madhusudan Ojha and T. Egami, *J. Phys.: Condens. Matter.* **25**, 435505 (2013).
34. T. Egami, S. J. Poon, Z. Zhang and V. Keppens, *Phys. Rev. B* **76**, 024203 (2007).
35. J. R. Morris, R. S. Aga, V. Levashov and T. Egami, *Phys. Rev. B* **77**, 174201 (2008).
36. C. W. Ryu and T. Egami, *Phys. Rev. E* **102**, 042615 (2020).
37. C. A. Angell, *Science* **267**, 1924 (1995).
38. H. Kato, T. Wada, M. Hasegawa, J. Saida, A. Inoue, and H. S. Chen, *Scr. Mater.* **54**, 2023 (2006).

39. N. Chen, Y. Li, and K. F. Yao, *J. Alloys Compd.* **504**, S211 (2010).
40. A. Jaiswal, T. Egami, K. F. Kelton, K. S. Schweizer, and Y. Zhang, *Phys. Rev. Lett.* **117**, 205701 (2016).
41. W. L. Johnson, J. H. Na, and M. D. Demetriou, *Nat. Commun.* **7**, 10313 (2016).
42. J. C. Qiao, R. Casalini, and J. M. Pelletier, *J. Non-Cryst. Solids* **407**, 106 (2015).
43. T. Komatsu, *J. Non-Cryst. Solids* **185**, 199 (1995).
44. L. Berthier and W. Kob, *Phys. Rev. E* **85**, 011102 (2012).
45. S. Alexander and J. P. McTague, *Phys. Rev. Lett.* **41**, 702 (1978).
46. S. Sachdev and D. R. Nelson, *Phys. Rev. B* **32**, 4592 (1985).
47. D. B. Miracle, *Nature Mater.* **3**, 697 (2004).
48. H. W. Sheng, W. K. Luo, F. M. Alamgir, J. M. Bai and E. Ma, *Nature*, **439**, 419 (2006).
49. C. P. Royall and S. R. Williams, *Phys. Rep.* **560**, 1 (2015).
50. D. Srolovitz, K. Maeda, V. Vitek and T. Egami, *Philos. Mag. A* **44**, 847 (1981).
51. T. Iwashita, D. M. Nicholson and T. Egami, *Phys. Rev. Lett.* **110**, 205504 (2013).
52. M. E. Blodgett, T. Egami, Z. Nussinov and K. F. Kelton, *Scientific Reports* **5**, 13837 (2015).
53. A. Jaiswal, T. Egami, K. F. Kelton, K. S. Schweizer and Y. Zhang, *Phys. Rev. Lett.* **117**, 205701 (2016).

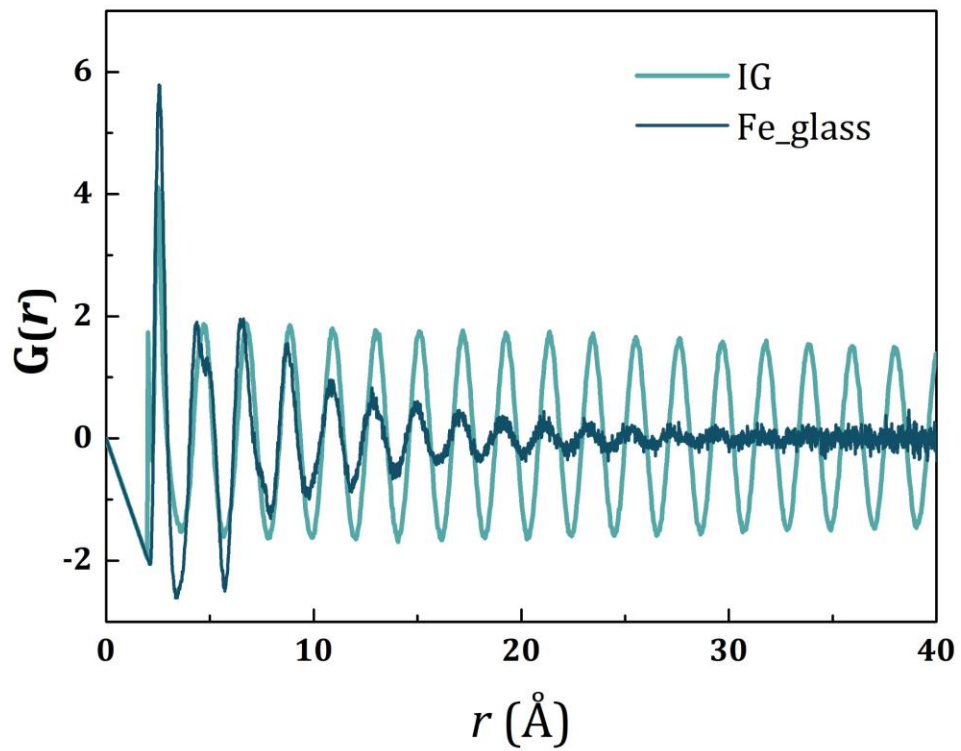


Fig. 1 The reduced PDF,  $G(r)$ , of Fe glass at  $T_g$  (dark curve), and  $G(r)$  of the structurally coherent ideal Fe glass obtained by the RMC method (light curve).

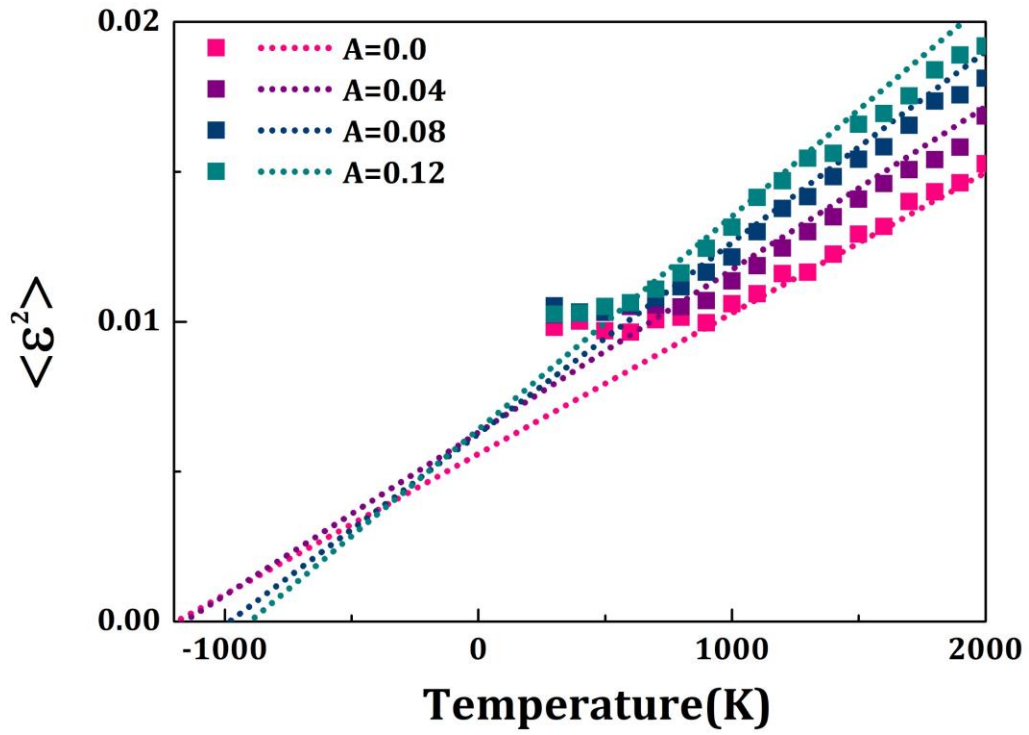


Fig. 2 The MRO strain,  $\langle \varepsilon_v^2 \rangle = (9/10\pi^3)(a/\xi_s)$ , for liquid Fe with various values of A (symbols), and by eq. (27) (dotted lines).

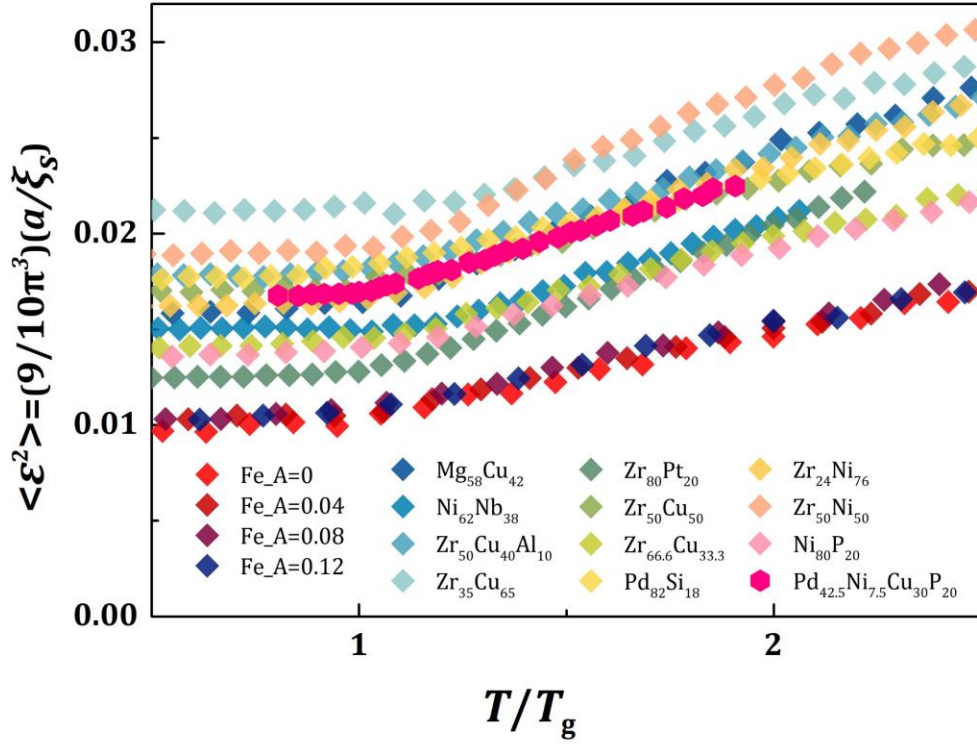
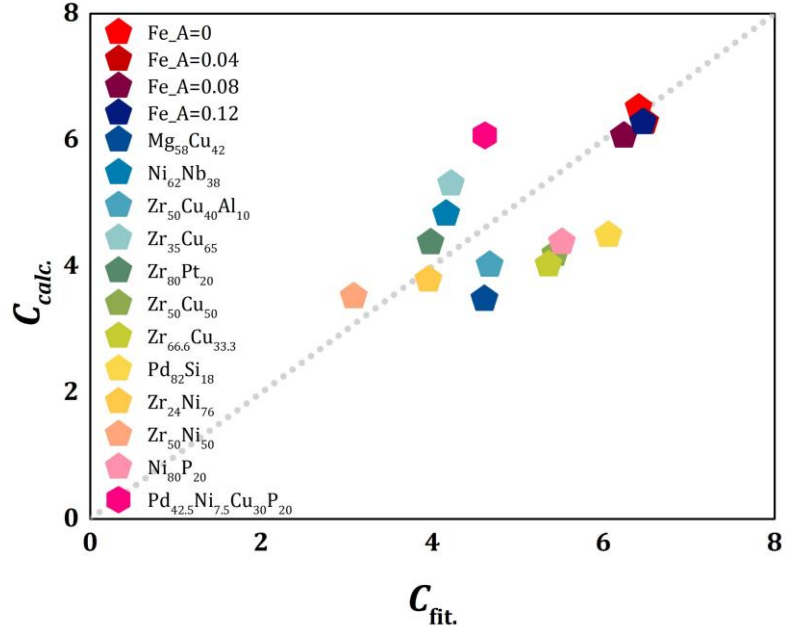
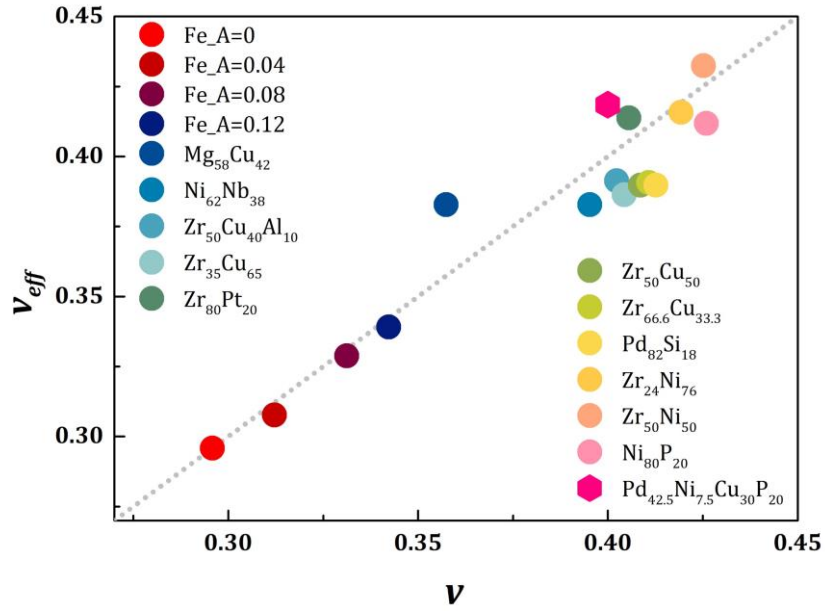


Fig. 3 The MRO strain related to the structural coherence length,  $\langle \varepsilon_v^2 \rangle = (9/10\pi^3)(a/\xi_s)$ , for Pd<sub>42.5</sub>Ni<sub>7.5</sub>Cu<sub>30</sub>P<sub>20</sub> alloy liquid determined by x-ray diffraction, and for various metallic alloy liquids obtained by simulation [13].



(a)



(b)

Fig. 4 (a) The value of  $C$  in eq. (29) determined for the data in Fig. 2 and S1, compared to the calculation by eq. (30), (b) The effective Poisson's ratio,  $\nu_{eff}$ , obtained by fitting eq. (27) to the data, compared to the calculated values of  $\nu$ . The line indicates  $\nu_{eff} = \nu$ .

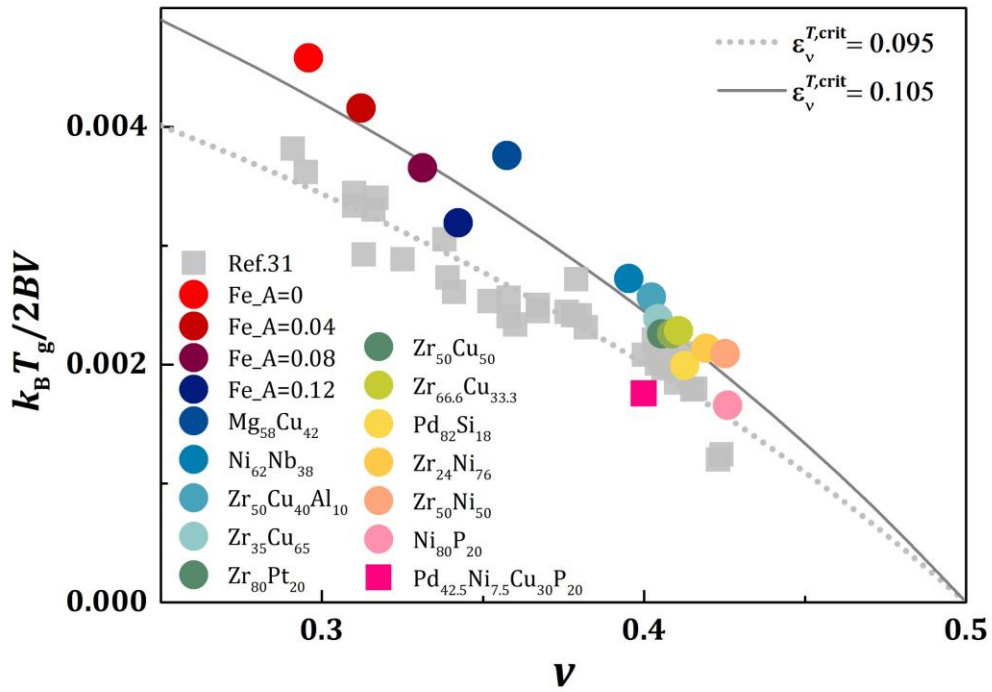


Fig. 5  $k_B T_g / 2BV$  plotted against Poisson's ratio,  $\nu$ . Circles are for simulation (this work) and squares are for experimental values by Ref. 34. Lines are for two values of  $\epsilon_v^{T,crit}$  by eq. (33).

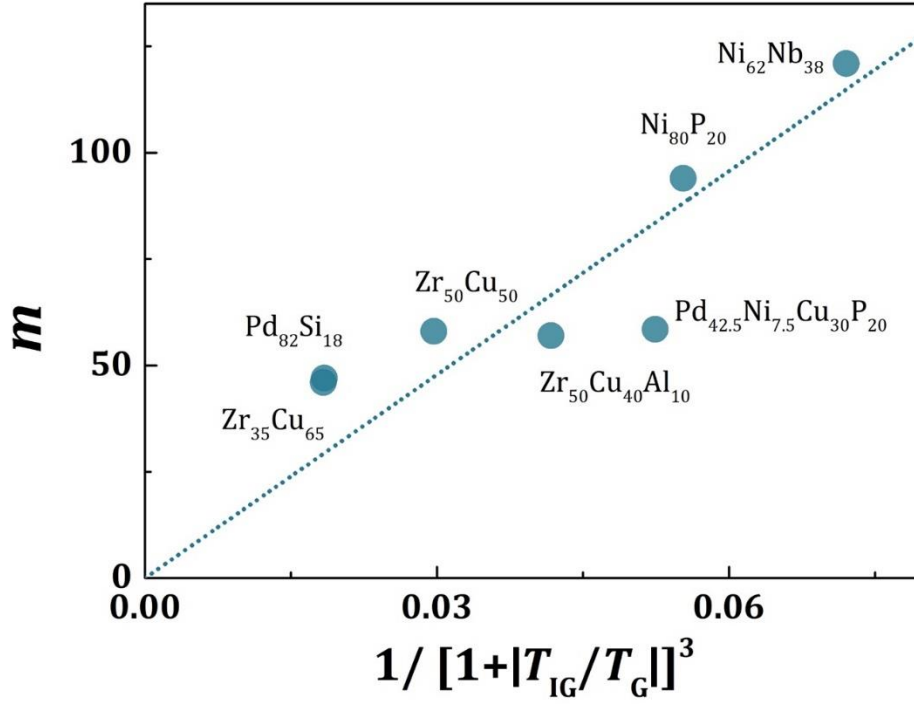


Fig. 6 Fragility coefficient,  $m$ , determined by experiment ( $Pd_{42.5}Ni_{7.5}Cu_{30}P_{20}$  [38],  $Pd_{82}Si_{18}$  [39],  $Zr_{35}Cu_{65}$  [40],  $Zr_{50}Cu_{50}$  [41],  $Zr_{50}Cu_{40}Al_{10}$  [42],  $Ni_{62}Nb_{38}$  [43],  $Ni_{80}P_{20}$  [41]) compared to  $1/[1 + |T_{IG}/T_g|]^3$ . The  $|T_{IG}/T_g|$  is related to the magnitude of the misfit strain through eq. (42).